An all-silicon, single-mode Bragg cladding rib waveguide

Ee Jin Teo[1,*], Andrew A. Bettiol[1], Boqian Xiong[1], Mark B. H. Breese[1], and Prashant T. Shuvan[2]

[1]Centre for Ion Beam Applications (CIBA), Department of Physics, 2 Science Drive 3, National University of Singapore, 117542, Singapore
[2]Department of Physics, Sri Sathya Sai University, Prasanthi Nilayam 515134 AP, India
**phytej@nus.edu.sg*

Abstract: In this paper, we demonstrate a direct method of fabricating an all-silicon, single-mode Bragg cladding rib waveguide using proton beam irradiation and subsequent electrochemical etching. The Bragg waveguide consists of porous silicon layers with a low index core of 1.4 that is bounded by eight bilayers of alternating high and low refractive index of 1.4 and 2.4. Here, the ion irradiation acts to reduce the thickness of porous silicon formed, creating an optical barrier needed for lateral confinement. Single-mode guiding with losses as low as approximately 1 dB/cm were obtained for both TE and TM polarization over a broad range of wavelengths from 1525 nm to 1625 nm. Such an approach offers a method for monolithic integration of Bragg waveguides in silicon, without the need for multiple processes of depositing alternating materials.

OCIS codes: (230.7370) Waveguides; (160.3130) Integrated Optics Materials; (130.5990) Semiconductor material; (130.3060) Infrared.

References and Links

1. S. Y. Lin, E. Chow, V. Hietala V, P. R. Villeneuve, and J. D. Joannopoulos, "Experimental demonstration of guiding and bending of electromagnetic waves in a photonic crystal," Science **282**(5387), 274–276 (1998).
2. E. Yablonovitch, "Inhibited spontaneous emission in solid-state physics and electronics," Phys. Rev. Lett. **58**(20), 2059–2062 (1987).
3. J. C. Knight, J. Broeng, T. A. Birks, and P. S. J. Russell, "Photonic band gap guidance in optical fibers," Science **282**(5393), 1476–1478 (1998).
4. H. Schmidt, Dongliang Yin, J. P. Barber, and A. R. Hawkins, "Hollow-core waveguides and 2-D waveguide arrays for integrated optics of gases and liquids," IEEE J. Sel. Top. Quantum Electron. **11**(2), 519–527 (2005).
5. B. Temelkuran, S. D. Hart, G. Benoit, J. D. Joannopoulos, and Y. Fink, "Wavelength-scalable hollow optical fibres with large photonic bandgaps for CO_2 laser transmission," Nature **420**(6916), 650–653 (2002).
6. P. Yeh, A. Yariv, and E. Marom, "Theory of Bragg fiber," J. Opt. Soc. Am. **68**(9), 1196 (1978).
7. P. Yeh, Optical Waves in Layered Media (Wiley, New York, United States 1988)
8. Y. Fink, J. N. Winn, S. Fan, C. Chen, J. Michel, J. D. Joannopoulos, and E. L. Thomas, "A dielectric omnidirectional reflector," Science **282**(5394), 1679–1682 (1998).
9. J. N. Winn, Y. Fink, S. Fan, and J. D. Joannopoulos, "Omnidirectional reflection from a one-dimensional photonic crystal," Opt. Lett. **23**(20), 1573–1575 (1998).
10. M. Ibanescu, Y. Fink, S. Fan, E. L. Thomas, and J. D. Joannopoulos, "An all-dielectric coaxial waveguide," Science **289**(5478), 415–419 (2000).
11. Y. Yi, S. Akiyama, P. Bermel, X. Duan, and L. C. Kimerling, "On-chip Si-based Bragg cladding waveguide with high index contrast bilayers," Opt. Express **12**(20), 4775–4780 (2004).
12. L. Pavesi, "Porous silicon dielectric multilayers and microcavities," Riv. Nuovo Cim. **20**(10), 1–76 (1997).
13. A. Bruyant, G. Lerondel, P. J. Reece, and M. Gal, "All-silicon omnidirectional mirrors based on one-dimensional photonic crystals," Appl. Phys. Lett. **82**(19), 3227 (2003).
14. E. Xifré-Pérez, L. F. Marsal, J. Ferré-Borrull, and J. Pallarès, "Porous silicon omnidirectional mirrors and distributed Bragg reflectors for planar waveguide applications," J. Appl. Phys. **102**(6), 063111 (2007).
15. E. J. Teo, M. B. H. Breese, A. A. Bettiol, D. Mangaiyarkarasi, F. Champeaux, F. Watt, and D. J. Blackwood, "Multicolour Photoluminescence from Porous Silicon using Focused High-energy Helium Ions," Adv. Mater. **18**(1), 51–55 (2006).
16. D. Mangaiyarkarasi, M. B. H. Breese, Y. S. Ow, and C. Vijila, "Controlled blueshift of the resonant wavelength in porous silicon microcavities using ion irradiation," Appl. Phys. Lett. **89**(2), 021910 (2006).
17. E. J. Teo, M. B. H. Breese, E. P. Tavernier, A. A. Bettiol, F. Watt, M. H. Liu, and D. J. Blackwood, "Three-dimensional microfabrication in bulk silicon using high-energy protons," Appl. Phys. Lett. **84**(16), 3202 (2004).

#124855 - $15.00 USD Received 1 Mar 2010; revised 8 Apr 2010; accepted 11 Apr 2010; published 13 Apr 2010

18. M. B. H. Breese, F. J. T. Champeaux, E. J. Teo, A. A. Bettiol, and D. Blackwood, "Hole transport through proton-irradiated p-type silicon wafers during electrochemical anodisation," Phys. Rev. B **73**(3), 035428 (2006).
19. D. E. Aspnes, "Optical properties of thin films," Thin Solid Films **89**(3), 249–262 (1982).
20. D. Mangaiyarkarasi, M. B. H. Breese, and Y. S. Ow, "Fabrication of three dimensional porous silicon distributed Bragg reflectors," Appl. Phys. Lett. **93**(22), 221905 (2008).
21. http://www.rsoftdesign.com
22. A. A. Bettiol, S. Venugopal Rao, E. J. Teo, J. A. van Kan, and F. Watt, "Fabrication of buried channel waveguides in photosensitive glass using proton beam writing," Appl. Phys. Lett. **88**(17), 171106 (2006).
23. P. Pirasteh, J. Charrier, Y. Dumeige, S. Haesaert, and P. Joubert, "Optical loss study of porous silicon and oxidized porous silicon planar waveguides," J. Appl. Phys. **101**(8), 083110 (2007).
24. V. Lehmann, F. Hofmann, F. Moller, and U. Gruing, "Resistivity of porous silicon: a surface effect," Thin Solid Films **255**(1-2), 20–22 (1995).
25. G. Z. Mashanovich, M. Milosevic, P. Matavulj, S. Stankovic, B. Timotijevic, P. Y. Yang, E. J. Teo, M. B. H. Breese, A. A. Bettiol, and G. T. Reed, "Silicon photonic waveguides for different wavelength regions," Semicond. Sci. Technol. **23**(6), 064002 (2008).
26. R. A. Soref, S. J. Emelett, and W. R. Buchwald, "Silicon waveguided components for the long-wave infrared region," J. Opt. A, Pure Appl. Opt. **8**(10), 840–848 (2006).

1. Introduction

Much progress has been made in recent times in the use of periodic dielectric structures with high refractive index contrast for waveguiding applications. Specific examples include two dimensional slab waveguides where lateral light confinement is achieved by a photonic crystal [1,2], and optical fibers that confine light to a low index core by virtue of a periodic glass cladding [3], the so called 'holey fibers'. In both examples, light is confined by a photonic band gap rather than total internal reflection. Such structures allow for the possibility of light being guided in a core region that has a lower refractive index than the surrounding cladding material. In the case of optical fiber, air guiding is made possible enabling high power transmission with zero dispersion and material absorption. Important applications of such fibers include gas and liquid sensing [4] and high power laser surgery [5].

Another example of a periodic dielectric structure that can be used for light guiding is the Bragg mirror. The Bragg mirror is a one dimensional periodic structure made from alternating layers of high and low refractive index material. The stop band for such a structure can be easily tuned by choosing the thickness and refractive index of each layer. Using a Bragg mirror for light guiding was first proposed by Yeh et. al. [6,7] and later realized by Fink et. al. [8] and Winn et. al. [9]. An example of such a structure is the omniguide, which utilizes concentric high index contrast dielectric layers as an omnidirectional (OM) mirror, to enhance mode confinement in the low index core [10]. Fabrication of these structures is less stringent on the resolution of the patterning process, since they do not require sub-micron periodicity in all three orthogonal directions. However, this design is difficult to implement on a silicon chip. Recently, Yi et. al. [11] demonstrated Bragg waveguides in silicon by depositing multilayers of alternating Si and Si_3N_4 layers on an alternative structure using CMOS technologies.

In this work, we make use of porous silicon (PS) technology to fabricate omnidirectional waveguides monolithically on to a silicon chip. By varying the current density during electrochemical etching, the refractive index can be tuned over a wide range of values from 1.2 to 3. The thickness of each PS layer can also be independently controlled by varying the etching time [12]. Due to the self-limiting process of PS formation, alternating layers of high and low index can be grown in a single etching step. This eliminates the multiple steps of depositing alternating materials using several deposition processes. We also employ an ion beam irradiation step to provide a means for laterally confining light. Although OM mirrors have been demonstrated using PS [13], prospects for waveguiding has only been proposed theoretically by Xifre-Perez et. al. [14]. Here, we aim to extend this theoretical analysis to provide fabrication method for the experimental realization of such a structure.

2. Experiment

In order to fabricate rib waveguides with multilayered porous silicon cladding we employed a patterning process that utilizes a focused beam of mega-electron volt protons. This process

#124855 - $15.00 USD Received 1 Mar 2010; revised 8 Apr 2010; accepted 11 Apr 2010; published 13 Apr 2010

has previously been used to form PS with spatially varying photoluminescence emission [15] and distributed Bragg reflectors that have varying reflectivity [16]. Here, two closely spaced lines are selectively irradiated with a focused beam of 2 MeV protons into a bulk Si wafer with a resistivity of 0.02 Ω.cm, in order to create an optical barrier needed for lateral confinement (Fig. 1). The ion irradiation acts to increase the local resistivity of the silicon, reducing the rate of PS formation in the irradiated regions during subsequent anodization with alternating high and low current density [17,18]. The resultant structure resembles a Bragg cladding rib waveguide with thinner layers at both sides of the core region. As the patterning occurs before the PS formation, the integrity of the PS is preserved.

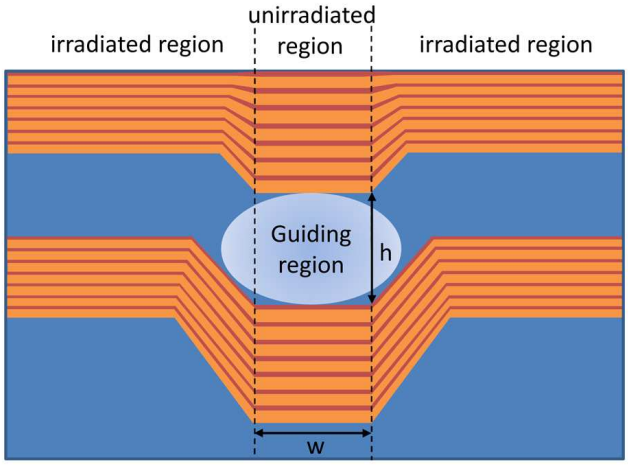

Fig. 1. Schematic diagram of the fabrication process

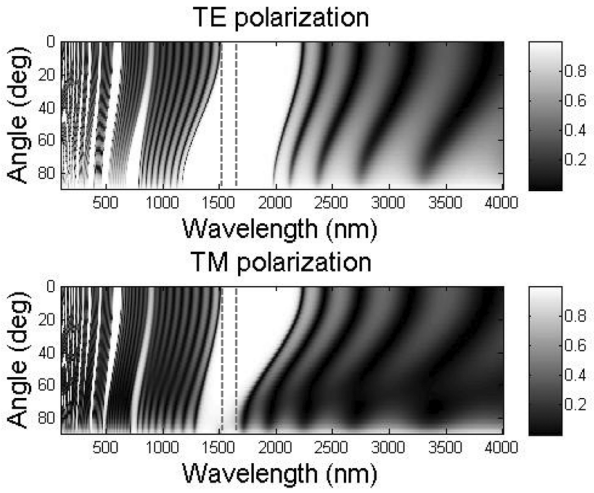

Fig. 2. Surface plots of the simulated reflectance of the Bragg reflectors as a function of wavelength and angles, in TE and TM polarizations.

In order to optimize the waveguide design for guiding at 1550 nm, we simulated the reflectivity from the Bragg reflector for a large range of angles and polarization using the transfer matrix method. Since the waveguide modes approaches the layers at glancing angle, the quarter-wave condition has to be modified for glancing angle incidence. It is found that optimum values occurs at about $d_h/d_h + d_l = 0.44$, where d_h and d_l are the thickness of the high and low refractive index layer [14]. The results shown in Fig. 2 are for eight bilayers with

#124855 - $15.00 USD Received 1 Mar 2010; revised 8 Apr 2010; accepted 11 Apr 2010; published 13 Apr 2010

thicknesses of 300 nm and 200 nm, and refractive indices of 1.40 and 2.38 respectively. The dotted lines in Fig. 2 demarcate the wavelength range where omnidirectional reflectivity occurs. In this case this occurs over a ~100 nm wavelength range from 1480 nm to 1680 nm, covering the C + L communications band. The actual refractive index of the fabricated structure was determined from fitting the reflectance spectrum using the Bruggeman model for the PS dispersion relation [19]. Although omnidirectionality is not necessary for guiding, it enhances confinement and is correlated to the polarization independent large band gap [14].

3. Results

The fabricated waveguide structures consist of a central core layer of 1.4 index that is bounded by eight bilayers of alternating high and low index of 2.4 and 1.4. Figure 3(a) and 3(b) show the cross-sectional SEM images of the waveguides with a core width and height of 3 × 4 μm, irradiated using a fluence of 2×10^{15} protons/cm^2 and 4×10^{15} protons/cm^2 respectively. The alternating high and low index of the bilayers corresponds to the bright and dark contrast lines respectively. We can observe from these images that the thickness of the PS layers reduces with ion fluence, resulting in an increase in the sidewall angles and the displacement between the two regions. At the intermediate regions where the thicker layer tapers towards the thinner irradiated region, a chirping effect is produced (Fig. 4). Previous studies have shown that chirping widens the reflectance band gap, which is important for stronger light confinement in the low index core [20]. In this case, the uniform damage profile of 2 MeV protons for the first ~40 μm is important for maintaining a constant slower PS growth rate over the range of the device layer.

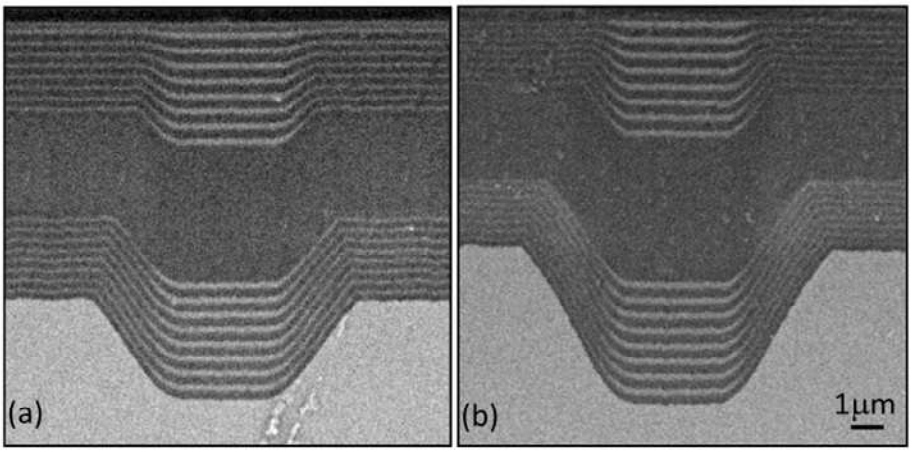

Fig. 3. (a) and (b) shows the cross sectional SEM image of Bragg cladding waveguide irradiated with a fluence of 2×10^{15}/cm^2 and 4×10^{15}/cm^2.

#124855 - $15.00 USD Received 1 Mar 2010; revised 8 Apr 2010; accepted 11 Apr 2010; published 13 Apr 2010

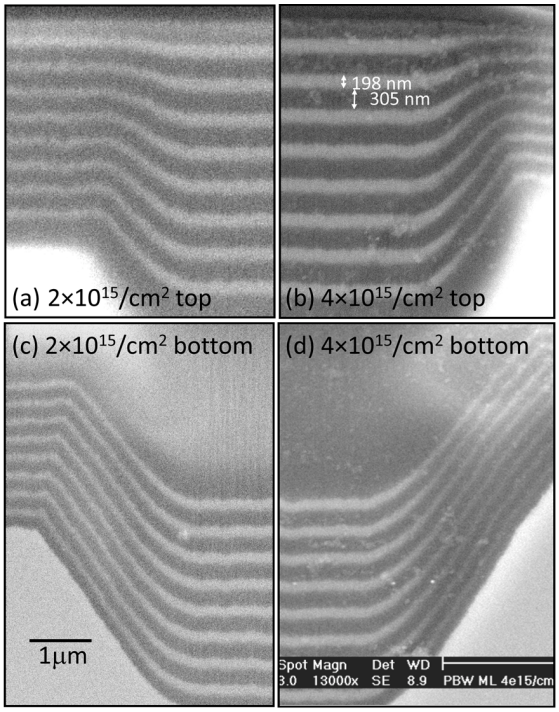

Fig. 4. show the close-up SEM images of the top and bottom claddings of the waveguide sidewalls for a fluence of 2×10^{15}/cm^2 and 4×10^{15}/cm^2 respectively.

The Finite Element Method (FEM) was used to simulate the fundamental mode field diameter and single-mode condition supported by the proton written structures at a free space wavelength of 1.55 μm. This software allows the number of guided modes to be found for an arbitrary structure with high index contrast [21]. Each grid can be subdivided into triangular segments using the non-uniform meshing feature in order to better conform to the index profile at the slanted edges of the sidewalls. We were able to accurately model the waveguide geometry for each fluence by incorporating a compression factor and a rate of change of sidewall angle with depth as observed in Fig. 3 and 4. Figure 5 shows the cross sectional profile of the simulated design for 2×10^{15} protons/cm^2 and 4×10^{15} protons/cm^2. It can be seen from this image that most of the power is confined in the low index core for both structures, and the corresponding fundamental TE and TM modes can be seen from the distribution of the electric field components in the x and y direction. It is also apparent that the TE mode is larger than the TM mode, since it is less confined in the lateral direction. According to simulations of the 1/*e* electric field width for the fundamental mode profile [Fig. 6(a)], the TE mode spot size is slightly larger (about 0.1 μm) than the TM mode for both fluences. As the sidewalls of the top and bottom cladding gets sharper, this closes the gap where the modes can leak out and increases the light confinement within the Bragg mirrors. We can see a remarkable decrease in mode size in both TE and TM polarizations. Simulations show that the mode field diameter for the higher fluence irradiation are about 1 μm smaller than the lower irradiated ones for a given core width. This is useful for designing waveguide bends with a smaller radius of curvature.

#124855 - $15.00 USD Received 1 Mar 2010; revised 8 Apr 2010; accepted 11 Apr 2010; published 13 Apr 2010

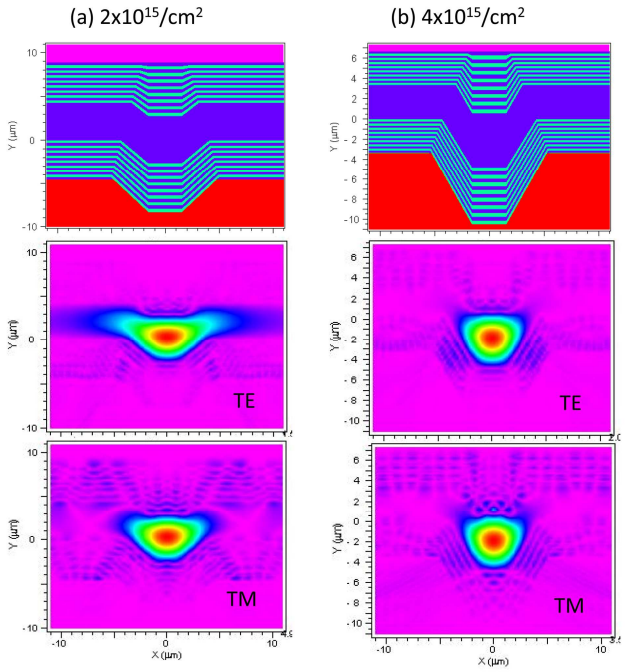

Fig. 5. (a) and (b) show the simulated structure and their corresponding fundamental TE and TM modes for 2×10^{15} and $4 \times 10^{15}/\text{cm}^2$.

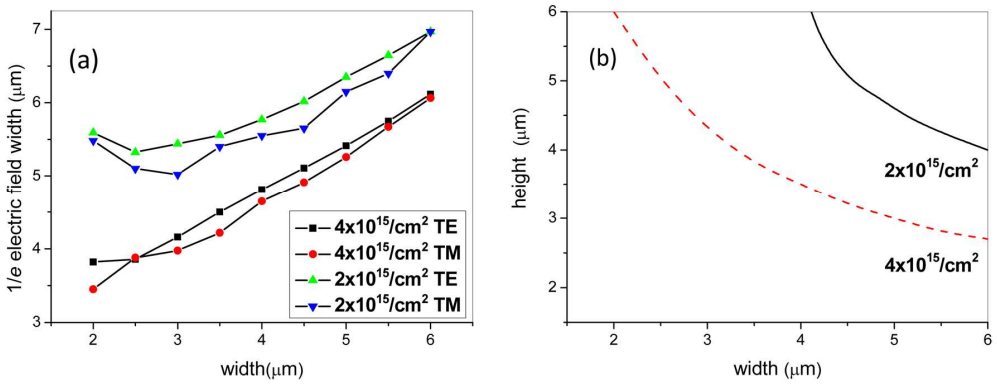

Fig. 6. (a) shows the plot of 1/*e* electric field width as a function of width in TE and TM polarizations. Figure 6(b) shows the theoretical single-mode boundary as the width and height of the core is varied.

Figure 6(b) shows a series of simulations where both the width and height of the core has been varied. The lines plotted indicate the boundary between single-mode and multimode for 2×10^{15} protons/cm^2 and 4×10^{15} protons/cm^2 waveguide designs, whereby regions below and to the left of the lines shows single-mode in both polarizations. Single-mode guiding can be supported by large cores of several microns in width and height, and the boundary is found to shift further upwards for lower fluence. Since the higher order modes become more confined by the sharper sidewalls of the higher irradiated structure, a smaller core size is needed for single-mode operation. As the height increases beyond 7 μm, no guiding is observed in the TE polarization for the 2×10^{15} protons /cm^2 waveguide design. The structure behaves like a planar waveguide and light can no longer be laterally confined.

#124855 - $15.00 USD Received 1 Mar 2010; revised 8 Apr 2010; accepted 11 Apr 2010; published 13 Apr 2010

Propagation losses were measured using the scattered light technique [22]. A 30 mW C + L broadband source (1525-1625 nm) is coupled into the waveguide using a 60 × objective. A cube polarizing beamsplitter and half waveplate are inserted into the beam path, enabling discrimination between TE and TM polarizations. Light scattered from the top of the waveguides is collected using a microscope coupled to a highly sensitive peltier cooled InGaAs camera (Xeva-FPA-1.7-320). Uncertainty in the loss data is determined from statistical fluctuations of five independent waveguide measurements. Figure 7 shows the scattered light intensity in dB over a length of 1 cm. Images are recorded away from the edges in order to avoid edge scattering effects. Both waveguides fall into the single-mode regimes since they have a core width and height of 3 × 4 μm. For a fluence of 2×10^{15} protons/cm^2, losses of 0.9 ± 0.1 dB/cm and 0.7 ± 0.1 dB/cm are obtained for TE and TM polarizations respectively. The scattered light for the TE polarization exhibits higher intensity and broader width when compared to the TM polarization. At a higher fluence of 4×10^{15}protons/cm^2, the propagation loss increases to 2.8 ± 0.1 dB/cm and 2.5 ± 0.1 dB/cm for TE and TM polarizations. Although the higher irradiated structure has sharper sidewalls to provide better lateral confinement, the modes suffers from more interaction with the sidewalls and light leakage through the thinner bilayers formed with higher fluence. This can be seen from the simulations in Fig. 5, which can account for the higher loss values obtained.

In order to reduce the propagation loss, it is important to determine the sources of loss. This includes material absorption, scattering from interfaces (σ_{rms} ~9 nm) and nanocrystallites [23]. Free carrier absorption can account for the majority of propagation loss in these p^+ anodized waveguides. However, it is important to note that absorption in p^+ nanocrystalline Si is much lower than crystalline silicon due to trapping at surface states [24]. This means that increasing the porosity can reduce the free-carrier absorption of the nanocrystals in the core layer. Sidewalls roughness caused by beam intensity fluctuations of the direct writing process and mechanical vibration of the stage scanning also contributes to propagation loss. This fluctuation can be averaged out by scanning the pattern over a few times. Optimization of the waveguide design by increasing the core size and number of bilayers can further help reduce the loss [25].

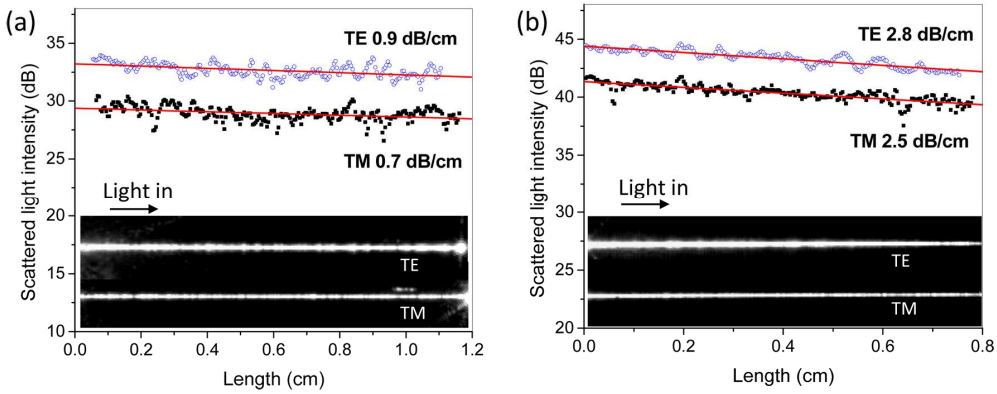

Fig. 7. shows the scattered light intensity as a function of length for (a) 2×10^{15}/cm^2 and (b) 4×10^{15}/cm^2 determined from the scattered light images in the inset.

4. Conclusion

We have demonstrated a direct method of fabricating single-mode Bragg cladding rib waveguide monolithically in silicon, without the need for multiple deposition processing steps. Our structures demonstrate low loss of 1-3 dB/cm in both TE and TM polarizations over a broad wavelength range of 1525-1625 nm. By accurately controlling the ion fluence at each region, it is possible to tune the waveguiding properties for optimal performance in a single patterning step. Larger single mode cores of several microns can be produced with

#124855 - $15.00 USD Received 1 Mar 2010; revised 8 Apr 2010; accepted 11 Apr 2010; published 13 Apr 2010

lower fluence, offering lower insertion loss and better mode matching with optical fibers. On the other hand, higher fluence produces structures with sharper sidewalls that supports smaller mode diameter, enabling better lateral confinement needed for guiding light around tight bends. Since these waveguides are fabricated entirely in silicon (oxide-free), tuning the Bragg cladding periodicity should result in low loss mid-infrared waveguiding [25,26]. Furthermore, the porous nature of these waveguides makes them also applicable for sensing applications. Currently, we are investigating on waveguide bends and results will be discussed in our future work.

Acknowledgements

The authors would like to acknowledge Melvin Fong for his contribution in the waveguide design and Isaac Ow for his helpful discussions. E. J. Teo gratefully acknowledged the financial assistance from Lee Kuan Yew Fellowship which is funded by Faculty of Research Council Startup Fund (WBS No. R-144-000-230-112).

#124855 - $15.00 USD Received 1 Mar 2010; revised 8 Apr 2010; accepted 11 Apr 2010; published 13 Apr 2010